



<b>Title</b>	<b>Copper aluminate spinel in the stabilization and detoxification of simulated copper-laden sludge</b>
<b>Author(s)</b>	<b>Tang, Y; Shih, K; Chan, K</b>
<b>Citation</b>	<b>Chemosphere, 2010, v. 80 n. 4, p. 375-380</b>
<b>Issued Date</b>	<b>2010</b>
<b>URL</b>	<b><a href="http://hdl.handle.net/10722/129127">http://hdl.handle.net/10722/129127</a></b>
<b>Rights</b>	<b>Creative Commons: Attribution 3.0 Hong Kong License</b>

1  
2 **Copper Aluminate Spinel in the Stabilization and Detoxification of Simulated**  
3 **Copper-Laden Sludge**

4  
5 Yuanyuan Tang, Kaimin Shih\*, King Chan

6  
7 Department of Civil Engineering, The University of Hong Kong, Pokfulam Road,  
8 Hong Kong, Hong Kong SAR, China

9  
10 \* Corresponding author. Tel: +852-28591973; fax: +852-25595337.

11 E-mail address: [kshih@hku.hk](mailto:kshih@hku.hk)

12  
13  
14 **Abstract**

15 This study aims to evaluate the feasibility of stabilizing copper-laden sludge by the  
16 application of alumina-based ceramic products. The processing temperature, material  
17 leaching behaviour, and the effect of detoxification were investigated in detail. CuO  
18 was used to simulate the copper-laden sludge and X-ray Diffraction was performed to  
19 monitor the incorporation of copper into the copper aluminate spinel ( $\text{CuAl}_2\text{O}_4$ ) phase  
20 in ceramic products. It was found that the development of  $\text{CuAl}_2\text{O}_4$  increased with  
21 elevating temperatures up to and including 1000 °C in the 3 h short sintering scheme.  
22 When the sintering temperature went above 1000 °C, the  $\text{CuAl}_2\text{O}_4$  phase began to  
23 decompose due to the high temperature transformation to  $\text{CuAlO}_2$ . The leachability  
24 and leaching behaviour of CuO and  $\text{CuAl}_2\text{O}_4$  were compared by usage of a prolonged  
25 leaching test modified from U.S. EPA's toxicity characteristic leaching procedure.  
26 The leaching results show that  $\text{CuAl}_2\text{O}_4$  is superior to CuO for the purpose of copper  
27 immobilization over longer leaching periods. Furthermore, the detoxification effect of  
28  $\text{CuAl}_2\text{O}_4$  was tested through bacterial adhesion with *Escherichia coli* K12, and the  
29 comparison of bacterial adhesion on CuO and  $\text{CuAl}_2\text{O}_4$  surfaces shows the beneficial  
30 detoxification effect in connection with the formation of the  $\text{CuAl}_2\text{O}_4$  spinel. This  
31 study demonstrates the feasibility of transforming copper-laden sludge into the spinel  
32 phase by using readily available and inexpensive ceramic materials, and achieving a  
33 successful reduction of metal mobility and toxicity.

34  
35 **Keywords:** Sludge; Spinel; Ceramic; Stabilization; Detoxification; Copper

36 **1. Introduction**

37

38 The discharge of hazardous metals into receiving waters is detrimental to human  
39 health and the environment. As a type of hazardous metal that is subject to potential  
40 bioaccumulation, copper may cause stomach and intestinal distress, liver and kidney  
41 damage, and anaemia in humans (Gardea-Torresdey et al., 1996). Copper is present in  
42 the wastewater generated from printed circuit board manufacturing, electroplating,  
43 wire drawing, copper polishing, paint production, wood preservatives and printing  
44 operations. Common strategies that are chosen to remove hazardous metals from  
45 wastewater include physicochemical processes such as precipitation, coagulation,  
46 reduction, ion exchange and membrane processes (Park et al., 2005). However, the  
47 treatments mentioned above always result in the production of large amounts of  
48 hazardous-metal bearing sludge which requires additional treatment.

49

50 At present, sludge with hazardous metal residues needs to be disposed of in  
51 controlled landfills. However, the high cost of this strategy, combined with the limited  
52 number of landfills capable of accepting highly toxic metal wastes, has made the  
53 development of effective and economical treatment technologies essential. Many  
54 investigators have attempted to immobilize toxic metals using sorbents or cements  
55 and then correlating the performance directly with metal leachability (Kapoor and  
56 Viraraghavan, 1996; Lin et al., 1998; Bailey et al., 1999). However,  
57 solidification/stabilization technologies via sorption or cementation mechanisms are  
58 not generally successful in the prevention of leaching in acidic environments, i.e. a pH  
59 value less than 4.0 (Bonen and Sarkar, 1995; Yousuf et al., 1995).

60

61 Based on phase transformation at high temperature, attempts to stabilize radioactive  
62 waste in vitrified glass or ceramic materials have been carried out through a variety of  
63 thermal treatments (Lewis et al., 1993; Lewis et al., 1994; Wronkiewicz et al., 1997;  
64 Wang et al., 2005; Shih and Leckie, 2007). However, the products are not reusable  
65 due to their radioactive nature. A similar thermal treatment process with relatively  
66 lower firing temperatures (900-1600 °C) compared to vitrification may be helpful in  
67 promoting the effective incorporation of waste materials into ceramic products, such  
68 as bricks, tiles, refractories, and aggregates (Teixeira da Silva et al., 1998; Shih and  
69 Leckie, 2007). Converting hazardous sludge to ceramic products via well-controlled  
70 thermal treatment can remove hazardous metals from the waste stream and enable  
71 them to become reusable. The leachability of hazardous metals can be reduced  
72 because of the change of mineral phase after thermal treatment. Shih et al. (2006a,  
73 2006b) successfully stabilized simulated nickel sludge by sintering with alumina,  
74 hematite and kaolinite as the ceramic raw materials. They reported significant  
75 reduction of nickel leachability from the spinel phases of the products, compared to  
76 the phase of nickel oxide.

77

78 It was previously reported that copper could be incorporated into the products  
79 sintered from clay materials, but the incorporation mechanism and phase  
80 transformation pathway have not been discussed in detail (Wei et al., 2001). An  
81 equilibrium phase diagram for  $\text{Cu}_2\text{O}-\text{Al}_2\text{O}_3$  system was published (Wartenberg and  
82 Reuch, 1935), and the formation of the copper spinel was obtained by calcining the  
83 co-precipitation mixture of copper and aluminium hydroxide (Gadalla and White,  
84 1964). Jacob and Alcock (1975) investigated the thermodynamics of copper aluminate  
85 spinel ( $\text{CuAl}_2\text{O}_4$ ) formation and delineated the equilibrium phase diagram of the

86 Cu<sub>2</sub>O-CuO-Al<sub>2</sub>O<sub>3</sub> system. The above equilibrium studies have provided a great  
87 opportunity to highlight the interaction between copper oxide and alumina at high  
88 temperatures. It is thus anticipated that the incorporation of copper-laden sludge into  
89 ceramic materials through thermal treatment may be a promising strategy for  
90 stabilizing hazardous copper wastes. However, the potential of initiating copper spinel  
91 formation in the industrial short-sintering scheme of ceramic products (i.e. tiles,  
92 insulators, refractories) will require further investigation.

93

94 As an environmentally benign product, the material's surface should be capable of  
95 supporting microbial activities. The adhesion of bacteria is usually the key factor for  
96 developing biofilm on material surfaces, which later becomes the major support basis  
97 for other biological growth. Due to the strong aquatic toxicity, copper oxide has been  
98 used in paints for marine environments to reduce the formation of biofilm on material  
99 surfaces. Copper-based paint may work as a selective medium for organisms by  
100 creating a toxic boundary layer at the surface as the component biocides leach out  
101 (Evans, 1981; Douglas-Helders et al., 2003). The use of copper-based paints to  
102 prevent biofilm development and a biofouling effect has gained increasing attention  
103 due to its environmental impact of releasing toxic copper ions into aquatic ecosystems  
104 (Chamberlain et al., 1988; Katranitsas et al., 2003). It has been reported that concrete  
105 sewer pipes coated with copper oxide exhibit antimicrobial characteristics and can  
106 achieve 99% inhibition against the bacterium (Hewayde et al., 2007). Toxicities of  
107 compounds can be measured singly and in mixtures of various complexities, using  
108 acute toxicity bioassays (Fernández-Alba et al., 2001, 2002). Recently, Xu et al. (2005)  
109 conducted a bacterium attachment study to evaluate the effectiveness of antifouling.  
110 Therefore, the density of bacteria adhering to product's surfaces may potentially be

111 used to evaluate the results of metal detoxification after the incorporation of  
112 hazardous copper waste into ceramics.

113

114 In this study, the effect of incorporating CuO, as the simulated copper-laden sludge,  
115 into  $\gamma$ -alumina ( $\gamma$ -Al<sub>2</sub>O<sub>3</sub>) ceramic precursors was observed under a short sintering  
116 process (3 h) with temperatures ranging 650-1150 °C. A prolonged leaching  
117 procedure similar to the toxicity characteristic leaching procedure (TCLP) was carried  
118 out to examine the stabilization effect of copper in the product phases. Whilst  
119 considering the toxic nature of CuO for microbial adhesion, the surfaces of CuO and  
120 the CuAl<sub>2</sub>O<sub>4</sub> were compared through bacterial adhesion experiment to evaluate the  
121 detoxification effect of producing the copper aluminate spinel in ceramics.

122

123

## 124 **2. Materials and Methods**

125

126 When thermally treated, the metal components of sludge are usually first  
127 transformed into oxide forms and thus CuO (Sigma Aldrich) was used to simulate the  
128 thermal reaction of copper-laden sludge. Experiments were carried out by firing the  
129 mixture of CuO and  $\gamma$ -Al<sub>2</sub>O<sub>3</sub> precursor. The  $\gamma$ -Al<sub>2</sub>O<sub>3</sub> was prepared from HiQ-7223  
130 alumina powder (Alcoa), which has a reported average particle size ( $d_{50}$ ) of 54.8 nm.  
131 The HiQ-7223 alumina was confirmed by X-ray Diffraction (XRD) to be the  
132 boehmite phase (AlOOH; ICDD PDF # 74-1875), and after heat treatment at 650 °C  
133 for 3 h it was successfully converted to  $\gamma$ -Al<sub>2</sub>O<sub>3</sub> with an XRD crystallite size of 2-5  
134 nm (Zhou and Snyder, 1991; Wang et al., 2005). The  $\gamma$ -Al<sub>2</sub>O<sub>3</sub> precursor and CuO  
135 were mixed to a total dry weight of 200 g at the Cu/Al molar ratio of 1:2, together

136 with 1 L of deionized water for ball milling of 18 h. The slurry samples were then  
137 dried and homogenized by mortar grinding. The derived powder was pressed into 20  
138 mm pellets at 650 MPa to ensure consistent compaction of the powder sample in  
139 readiness for the sintering process. After sintering, the samples were air-quenched and  
140 ground into powder for XRD analysis and the leaching test.

141

142 Phase transformations during sintering were monitored by XRD. The diffraction  
143 patterns were collected using a Bruker D8 diffractometer (Bruker Co. Ltd.) equipped  
144 with Cu X-ray tube operated at 40 kV and 40 mA. Scans were collected from 10 to  
145 90° 2 $\theta$ -angle, with a step size of 0.02° and a counting time of 1 s step<sup>-1</sup>. Phase  
146 identification was executed by matching XRD patterns with the powder diffraction  
147 files (PDF) database of the International Centre for Diffraction Data (ICDD). The  
148 leachability of the pure phase was tested using a leaching experiment which is a  
149 leaching procedure modified from the U.S. EPA SW-846 Method 1311 - Toxicity  
150 Characteristic Leaching Procedure (TCLP) with a pH 2.9 acetic acid solution  
151 (extraction fluid # 2) as the leaching fluid. Each leaching vial was filled with 10 mL  
152 of TCLP extraction fluid and 0.5 g of powder. The leaching vials were rotated end-  
153 over-end at 60 rpm for agitation periods of 0.75 to 22 d. At the end of each agitation  
154 period, the leachates were filtered with 0.2  $\mu$ m syringe filters, the pH was measured  
155 and the concentrations of all metals were derived from ICP-AES (Perkin-Elmer  
156 Optima 3300 DV).

157

158 In this study, the bacterial adhesion experiment was carried out to first qualitatively  
159 observe the toxicity of CuAl<sub>2</sub>O<sub>4</sub> surface. The *Escherichia coli* K12 bacteria strain was  
160 chosen for use in this adhesion evaluation on the surfaces of soda-lime glass (silica-

161 based),  $\text{CuAl}_2\text{O}_4$  and  $\text{CuO}$  pellets. The culture solution was prepared with 10 g of  
162 peptone bacteriological (Beijing Chemical Works, 44075-2H, 250 g), 10 g of  $\text{NaCl}$   
163 (Riedel-deHaen) and 5 g of yeast extract in 1 L of water. The glass material was taken  
164 from the microscope slides commonly designed for laboratory work, and it is an  
165 example of a non-toxic surface in the study of bacterial adhesion. The  $\text{CuO}$  powder  
166 was pressed into pellets and heated at  $950\text{ }^\circ\text{C}$  for 3 h. This was to effectively enhance  
167 the pellet strength and surface smoothness to facilitate the experimental needs, but  
168 also aimed to maintain the phase status ( $\text{CuO}$ ) of the material. The mixture of  $\text{CuO}$   
169 and  $\gamma\text{-Al}_2\text{O}_3$  powder ( $\text{Cu/Al}$  molar ratio = 1:2) was also pressed into pellets and heated  
170 until  $\text{CuAl}_2\text{O}_4$  was observed as the single phase in the product ( $990\text{ }^\circ\text{C}$  for 20 d). Both  
171  $\text{CuO}$  and  $\text{CuAl}_2\text{O}_4$  pellets derived from the above processes were later polished by the  
172 diamond lapping films progressively down to a diamond grit size of  $0.1\text{ }\mu\text{m}$ .  
173 Measurement of the surface roughness of glass,  $\text{CuO}$  and  $\text{CuAl}_2\text{O}_4$  samples was  
174 conducted using a JPK Instruments atomic force microscope (AFM) equipped by  
175 silicon-cantilevers with a force constant of  $0.1\text{ N m}^{-1}$  under the Cleveland method  
176 (Cleveland et al., 1993). Height images ( $40 \times 40\text{ }\mu\text{m}^2$ ) were used to calculate the  
177 roughness measurement based on the arithmetic average. Bacteria adhered on the  
178 substrata were stained with SYTO9 and observed using a fluorescence microscope  
179 (Nikon Eclipse E600).

180

181

### 182 **3. Results and Discussion**

183

#### 184 **3.1 Copper Spinel Formation**

185



186 By sintering the mixture of CuO and  $\gamma$ -Al<sub>2</sub>O<sub>3</sub>, copper incorporation may proceed  
187 under a recrystallization reaction as follows:

188



190

191 It has been reported that the incorporation ability of  $\gamma$ -Al<sub>2</sub>O<sub>3</sub> for nickel is affected  
192 by the sintering temperature (Shih et al., 2006a, 2006b). To investigate the effective  
193 temperature for alumina content to incorporate copper into the CuAl<sub>2</sub>O<sub>4</sub> in the  
194 practice of sintering construction ceramic products, a 3 h short sintering scheme at  
195 temperatures ranging from 650 to 1150 °C was conducted. According to the database  
196 of the CuAl<sub>2</sub>O<sub>4</sub> XRD pattern (ICDD PDF # 33-0448), its two major peaks are located  
197 at  $2\theta = 36.868$  and  $31.294^\circ$ , corresponding to the diffraction planes of (3 1 1) and (2 2  
198 0) respectively. The result reveals that the sample sintered at 750 °C developed a  
199 distinguishable CuAl<sub>2</sub>O<sub>4</sub> crystalline phase as shown in Fig. 1a. Jacob and Alcock  
200 (1975) observed the formation of the CuAl<sub>2</sub>O<sub>4</sub> in their equilibrium thermal experiment  
201 (for 24 h) and reported the spinel formation temperature to start at 612 °C. However,  
202 when compared to the results observed in our short sintering experiment, it was  
203 discovered that an effective sintering period for industrial application to incorporate  
204 copper into CuAl<sub>2</sub>O<sub>4</sub> in ceramic products should be at least above 750 °C. Since the  
205 solid state reaction is usually affected by both thermodynamic conditions and the  
206 diffusion process, this comparison may further suggest that spinel formation at  
207 temperatures below 750 °C is largely limited by the prevailing slow diffusion  
208 although it is thermodynamically feasible at temperatures above 612 °C. Below 750  
209 °C, the CuAl<sub>2</sub>O<sub>4</sub> phase formed by the short sintering scheme may only be limited at

210 the grain boundary of reactants, and the very small quantity of such phase in the  
211 system was not reflected in the XRD results.

212

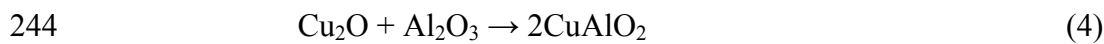
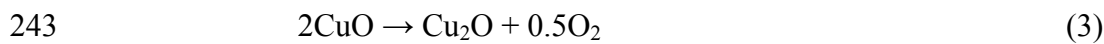
213 Two  $2\theta$  ranges of the XRD pattern ( $2\theta = 36.4\text{-}37.4^\circ$  and  $31.0\text{-}32.0^\circ$ ) were selected  
214 to further observe the peak intensity development to represent the  $\text{CuAl}_2\text{O}_4$  spinel  
215 product generated from the system at elevated temperatures (Fig. 2). Figure 2a  
216 observes the crystallization of  $\text{CuAl}_2\text{O}_4$  developed from the  $\text{CuO} + \gamma\text{-Al}_2\text{O}_3$  precursor  
217 within the  $2\theta$  range of  $36.4\text{-}37.4^\circ$  at different sintering temperatures. Although there  
218 was a distinguishable  $\text{CuAl}_2\text{O}_4$  phase in the  $750^\circ\text{C}$  sintered sample, the substantial  
219 growth of  $\text{CuAl}_2\text{O}_4$  in the system was observed to be at above  $850^\circ\text{C}$ , which may  
220 indicate the energy needed to overcome the major diffusion barrier in the system.  
221 Below  $1000^\circ\text{C}$ , the peak intensity of the  $\text{CuAl}_2\text{O}_4$  phase increases as the temperature  
222 increases. However, at sintering temperatures higher than  $1000^\circ\text{C}$ , the peak intensity  
223 of the  $\text{CuAl}_2\text{O}_4$  phase was found to decrease with elevated temperatures.

224

225 The XRD patterns within the  $2\theta$  range of  $31.0\text{-}32.0^\circ$  (Fig. 2b) show that the  
226 decrease of  $\text{CuAl}_2\text{O}_4$  at higher temperatures was due to the formation of another new  
227 Cu-Al oxide phase, cuprous aluminate delafossite ( $\text{CuAlO}_2$ ; ICDD PDF # 75-2356).  
228 Figure 2b has further verified the optimal formation temperature of  $\text{CuAl}_2\text{O}_4$  at  $1000^\circ\text{C}$ ,  
229 and the phase transformation to  $\text{CuAlO}_2$  at higher temperatures was observed by  
230 the (0 0 6) diffraction plane signal of  $\text{CuAlO}_2$  at  $2\theta$  around  $31.63^\circ$ . Since the decrease  
231 of  $\text{CuAl}_2\text{O}_4$  at higher temperatures was accompanied with a corresponding increase of  
232  $\text{CuAlO}_2$  in the system, it is suggested that the formation of  $\text{CuAlO}_2$  occurred  
233 immediately after the decomposition of  $\text{CuAl}_2\text{O}_4$ , or went through structural  
234 transformation by discharging the excessive aluminum and oxygen from the crystal

235 structure. Nevertheless, both phase transformation mechanisms indicate that the  
236 opportunity of immobilizing copper from the Al-O incorporated structures is small  
237 when this phase transformation process takes place at high temperatures. Together  
238 with the interaction between unreacted CuO and Al<sub>2</sub>O<sub>3</sub> (Jacob and Alcock, 1975), the  
239 CuAlO<sub>2</sub> formation mechanisms at temperatures above 1000 °C can be organized in  
240 the following way:

241



245

### 246 **3.2 The Leaching Mechanisms**

247

248 To investigate the effect of copper immobilization after the incorporation by the  
249 spinel structure, the preferred method was to first compare the leachability of single  
250 phase samples under the same leaching environment. Therefore, this study prepared a  
251 leaching experiment sample with CuAl<sub>2</sub>O<sub>4</sub> as the only phase appearing in the sample.  
252 From the incorporation efficiency experiment, it was observed that 1000 °C as the  
253 sintering temperature could attain the highest yield of CuAl<sub>2</sub>O<sub>4</sub> phase without  
254 initiating the formation of the CuAlO<sub>2</sub> phase, although small amounts of reactants  
255 (Al<sub>2</sub>O<sub>3</sub> and CuO) were still observed in the system. To ensure the complete  
256 transformation of reactants to the product phase (CuAl<sub>2</sub>O<sub>4</sub>), a longer sintering time  
257 (20 d) was used to facilitate reaction equilibrium. Moreover, the sintering temperature  
258 of 990 °C, which is slightly less than 1000 °C, was chosen to further prevent the  
259 generation of the CuAlO<sub>2</sub> phase during the prolonged sintering process. The XRD

260 pattern in Fig. 1b shows the success achieved by preparing the  $\text{CuAl}_2\text{O}_4$  sample,  
261 where no peak of  $\text{CuO}$  or  $\text{Al}_2\text{O}_3$  reactant phase was found in the pattern.

262

263 Samples used in the leaching test were ground into powder and measured to  
264 ascertain the BET surface area to yield values of  $1.35 \text{ m}^2 \text{ g}^{-1}$  for  $\text{CuAl}_2\text{O}_4$  and  $0.17 \text{ m}^2$   
265  $\text{g}^{-1}$  for  $\text{CuO}$ . The pH values are shown in Fig. 3a, which reveals the greater pH  
266 increase of  $\text{CuO}$  leachate. Within the first few days, the pH of  $\text{CuO}$  leachate  
267 experienced a significant increase which was then maintained at around 4.7-4.9  
268 throughout the rest of the leaching period. In contrast, the pH of the  $\text{CuAl}_2\text{O}_4$  leachate  
269 was maintained at the beginning value of its leaching fluid throughout the entire  
270 leaching period. The increase of leachate pH may arise due to the dissolution of  
271 cations through ion exchange with protons in the solution. This is accompanied by the  
272 destruction of crystals at the solid surface by the acidic leaching fluid. The increase in  
273 leachate pH may indicate that  $\text{CuO}$  is more vulnerable to proton-mediated dissolution.  
274 On the other hand,  $\text{CuAl}_2\text{O}_4$  (sintered from  $\gamma\text{-Al}_2\text{O}_3 + \text{CuO}$ ) may show higher intrinsic  
275 resistance to such acidic attack, even with higher surface areas.

276

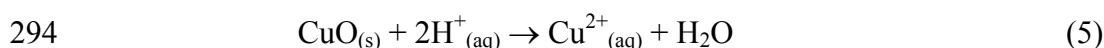
277 As the leaching for solid is likely dominated by surface reactions, it is expected to  
278 be proportional to sample surface area. In addition, since the same weight of sample  
279 (0.5 g) was always used, the total copper content in the sample, subject to the different  
280 copper phases, should also be normalized for comparison. Figure 4 summarizes the  
281 amounts of leached copper from samples normalized with respect to the surface areas  
282 of tested solids. The copper in the  $\text{CuO}$  leachate was over 400 times higher than that  
283 in the  $\text{CuAl}_2\text{O}_4$  leachate near the end of the leaching period. This confirms that the  
284  $\text{CuAl}_2\text{O}_4$  spinel phase has a higher intrinsic resistance to such acidic attack compared

285 to the CuO phase and the sintering strategy designed for copper-laden sludge is  
286 proven to be beneficial in stabilizing copper. The curve in the small diagram of Fig. 4  
287 further provides the details of copper concentrations in the CuAl<sub>2</sub>O<sub>4</sub> leachate.

288

289 When the pH of the CuO leachate reached ~ 4.9, the leaching of CuO stabilized at a  
290 copper concentration of ~ 2500 mg L<sup>-1</sup> (~ 10<sup>-1.4</sup> M) in the leachate. As a general  
291 assumption of cation-proton exchange mechanism, the destruction of copper oxide by  
292 the acidic attack of the solution can be expressed as:

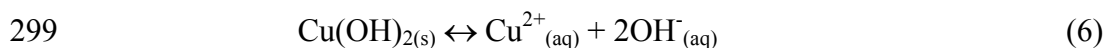
293



295

296 However, the concentration of copper ions in the solution [Cu<sup>2+</sup><sub>(aq)</sub>] is also limited  
297 by the potential precipitation/dissolution reactions, such as in respect to Cu(OH)<sub>2(s)</sub>:

298



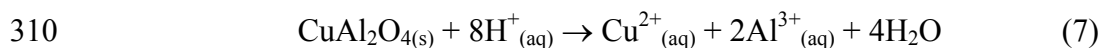
300

301 where the solubility constant (K<sub>sp</sub>) of Eq. 6 is 10<sup>-19.25</sup> (Stumm and Morgan, 1996). At  
302 pH 4.9, the product of [Cu<sup>2+</sup><sub>(aq)</sub>] × [OH<sup>-</sup><sub>(aq)</sub>]<sup>2</sup> was found to be 10<sup>-19.6</sup>, which is very  
303 close to the K<sub>sp</sub> of Cu(OH)<sub>2(s)</sub>. This result indicates that the system was very close to  
304 the saturation of Cu(OH)<sub>2(s)</sub> and the stabilization of copper concentration in the CuO  
305 leachate was likely controlled through the equilibrium with the Cu(OH)<sub>2(s)</sub> phase.

306

307 When leaching the CuAl<sub>2</sub>O<sub>4</sub> phase, a “congruent dissolution” through the cation-  
308 proton exchange reaction can be written as:

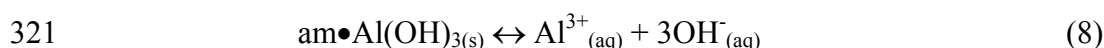
309



311

312 Such congruent dissolution would result in a theoretical  $[\text{Al}^{3+}_{(aq)}]/[\text{Cu}^{2+}_{(aq)}]$  molar  
 313 ratio of 2.0 in the leachates. However, this ratio was observed at 0.75-0.80 in the  
 314 leachate of  $\text{CuAl}_2\text{O}_4$  as shown in Fig. 3b. Since the system was maintained in a more  
 315 acidic environment ( $\sim \text{pH } 3.2$ ) and the copper concentration was much lower than that  
 316 of the  $\text{CuO}$  leachate, the copper concentrations in the leachates of  $\text{CuAl}_2\text{O}_4$  were all  
 317 considerably under-saturated regarding to the  $\text{Cu}(\text{OH})_{2(s)}$  phase. The aluminium  
 318 concentrations measured in the  $\text{CuAl}_2\text{O}_4$  leachates were  $\sim 9.5 \text{ mg L}^{-1}$  ( $\sim 10^{-3.45} \text{ M}$ ).  
 319 The reaction of amorphous aluminium hydroxide precipitation/dissolution is:

320



322

323 where the solubility constant ( $K_{sp}$ ) of Eq. 8 is  $10^{-32.7}$  (Stumm and Morgan, 1996). The  
 324 product of  $[\text{Al}^{3+}_{(aq)}] \times [\text{OH}^-_{(aq)}]^3$  was found to be  $10^{-35.9}$  and it did not reach the  
 325 saturation ( $[\text{Al}^{3+}_{(aq)}] \times [\text{OH}^-_{(aq)}]^3 = 10^{-32.7}$ ) of amorphous  $\text{Al}(\text{OH})_{3(s)}$  either. Therefore,  
 326 this suggests that the leaching behaviour of  $\text{CuAl}_2\text{O}_4$  in this experiment is likely to be  
 327 an incongruent dissolution, where the majority of the Al-O bonds still remained on the  
 328  $\text{CuAl}_2\text{O}_4$  spinel surface. Although some previous studies (Cailleateau et al., 2008;  
 329 Ohlin et al., 2010) have further suggested the reorganization of remaining molecules  
 330 in incongruent dissolution scenarios, the overall result indicates the existence of an  
 331 Al-rich layer on the leached  $\text{CuAl}_2\text{O}_4$  surface, which is beneficial for preventing the  
 332 further leaching of Cu and may increase product durability.

333

334 **3.3 Adhesion of *E. coli***

335

336 Since the density of bacteria adhering to the product surface may potentially be  
337 used to evaluate the results of metal detoxification, this study first conducted a  
338 qualitative comparison of bacterial adhesion on the substrata of the  $\text{CuAl}_2\text{O}_4$  spinel,  
339 CuO and soda-lime (silica-based) glass. Experimental studies have suggested the  
340 importance of the physicochemical and thermodynamic properties of both the  
341 substrata and the bacterial cell surface during the process of bacterial adhesion (Van  
342 Loosdrecht et al., 1989; Sjollem et al., 1990; Vadillo-Rodriguez and Logan, 2006).  
343 In this study, a type of testing bacteria, *E. coli* K12, was cultivated in a solution with a  
344 pH of  $\sim 6.5$  and all the substratum samples were collectively placed in the same  
345 solution for better comparison. Since surface roughness may impact bacterial  
346 adhesion (Brant and Childress, 2002), the tested surfaces of samples were polished  
347 using diamond lapping films and the roughness values were measured by AFM to be  
348  $2.3 \pm 1.7$ ,  $491 \pm 192$  and  $369 \pm 90$  nm for glass,  $\text{CuAl}_2\text{O}_4$  and CuO, respectively.

349

350 Figure 5 shows the results from the comparison of *E. coli* bacterial adhesion on the  
351 surface of glass,  $\text{CuAl}_2\text{O}_4$  and CuO after 18 h of bacterial cultivation. The amount of  
352 *E. coli* adhering to the glass surface visibly surpassed the amount on the surfaces of  
353 both the  $\text{CuAl}_2\text{O}_4$  and CuO samples (Fig. 5a). However, due to the toxicity effect, no  
354 bacterial adhesion was found on the surface of the CuO substratum as shown in the  
355 Fig. 5c. With much lower copper leachability as compared to CuO, the  $\text{CuAl}_2\text{O}_4$   
356 spinel clearly developed bacterial adhesion on the surface which showed its capacity  
357 to support microbial activities, although the level was lower than that of the glass  
358 substratum (Fig. 5b).

359

360 As the inhibition effect of copper oxide on biofouling has already been indicated  
361 (Evans, 1981; Balls, 1987; Chamberlain et al., 1988; Hodson and Burke, 1994;  
362 Douglas-Helders et al., 2003; Katranitsas et al., 2003; Hewayde et al., 2007), the  
363 comparison result of glass and CuO in this study is consistent with previous findings.  
364 Moreover, some studies suggested that the increase of nano-scale roughness of a  
365 surface increases bacterial adhesion (Shellenberger and Logan, 2002); other studies  
366 have demonstrated no significant relationship between surface roughness and bacterial  
367 adhesion (Li and Logan, 2004). In our work, the highest level of bacteria adhered to  
368 the glass surface, even with much lower roughness, thus indicating the dominant  
369 effect of substrata material. The growth of bacteria on the surface of the  $\text{CuAl}_2\text{O}_4$   
370 substratum suggests the successful detoxification of copper through the stabilization  
371 strategy of incorporating CuO into the aluminate spinel phase. Since the formation of  
372 a biofilm covering on a surface begins with the adhesion of a small number of bacteria,  
373 the results shown here provide direct evidence of the environmental friendliness of  
374 waste-incorporated ceramic products. Such information on the intrinsic properties of  
375 material is also important and beneficial when aiming to minimize the environmental  
376 impact even after the end of a product's life.

377

378

### 379 **Acknowledgements**

380

381 We acknowledge the funding for this research provided by the University of Hong  
382 Kong from its Research Seed Fund. The authors are thankful to Professor Xiang-Dong  
383 Li for providing the ICP-AES analysis. Dr. Tong Zhang, Mr. Yuanqing Chao and Ms.



384 Vicky Fung are thanked for assisting with the AFM technique and bacterial adhesion  
385 experiment.

386

## 387 **References**

388

389 Bailey, S.E., Olin, T.J., Bricka, R.M., Adrian, D.D., 1999. A review of potentially  
390 low-cost sorbents for heavy metals. *Water Res.* 33, 2469-2479.

391 Balls, P.W., 1987. Tributyltin (TBT) in the waters of a Scottish Sea Loch arising from  
392 the use of antifoulant treated netting by salmon farms. *Aquaculture* 65, 227-  
393 237.

394 Bonen, D., Sarkar, S.L., 1995. The effect of simulated environmental attack on  
395 immobilization of heavy metal doped in cement-based materials. *J. Hazard.*  
396 *Mater.* 40, 321-335.

397 Brant, J.A., Childress, A.E., 2002. Assessing short-range membrane-colloid  
398 interactions using surface energetics. *J. Membrane Sci.* 203, 257-273.

399 Cailleateau, C., Angeli, F., Devreux, F., Gin, S., Jestin, J., Jollivet, P., Spalla, O., 2008.  
400 Insight into silicate-glass corrosion mechanisms. *Nat. Mater.* 7, 978-983.

401 Chamberlain, A.H.L., Simmonds, S.E., Garner, B.J., 1988. Marine 'copper-tolerant'  
402 sulphate reducing bacteria and their effects on 90/10 copper-nickel (CA 706).  
403 *Int. Biodeterior.* 24, 213-219.

404 Cleveland, J.A., Manne, S., Bocek, D., Hansma, P.K., 1993. A nondestructive method  
405 for determining the spring constant of cantilevers for scanning force  
406 microscopy. *Rev. Sci. Instrum.* 64, 403-405.

407 Douglas-Helders, G.M., Tana, C., Carson, J., Nowak, B.F., 2003. Effects of copper-  
408 based antifouling treatment on the presence of *Neoparamoeba pemaquidensis*  
409 Page, 1987 on nets and gills of reared Atlantic salmon (*Salmo salar*).  
410 *Aquaculture* 221, 13-22.

411 Evans, L.V., 1981. Marine algae and fouling-a review, with particular reference to  
412 ship-fouling. *Bot. Mar.* 24, 167-171.

413 Fernández-Alba, A.R., Hernando, M.D., López, G.D., Chisti, Y., 2001. Toxicity of  
414 pesticides in wastewater: a comparative assessment of rapid bioassays. *Anal.*  
415 *Chim. Acta* 426, 289-301.

416 Fernández-Alba, A.R., Hernando, M.D., López, G.D., Chisti, Y., 2002. Toxicity  
417 evaluation of single and mixed antifouling biocides measured with acute  
418 toxicity bioassays. *Anal. Chim. Acta* 456, 303-312.

419 Gadalla, A.M.M., White, J., 1964. Equilibrium relationships in the system CuO-  
420 Cu<sub>2</sub>O-Al<sub>2</sub>O<sub>3</sub>. *J. Brit. Ceram. Soc.* 63, 39-62.

421 Gardea-Torresdey, J.L., Tang, L., Salvador, J.M., 1996. Copper adsorption by  
422 esterified and unesterified fractions of Sphagnum peat moss and its different  
423 humic substances. *J. Hazard. Mater.* 48, 191-206.

424 Hewayde, H., Nakhla, G.F., Allouche, E.N., Mohan, P.K., 2007. Beneficial impact of  
425 coatings on biological generation of sulphide in concrete sewer pipes. *Struct.*  
426 *Infrastruct. E.* 3, 267-277.

427 Hodson, S.L., Burke, C., 1994. Microfouling of salmon-cage netting: a preliminary  
428 investigation. *Biofouling* 8, 93-105.

429 Jacob, K.T., Alcock, C.B., 1975. Thermodynamics of CuAlO<sub>2</sub> and CuAl<sub>2</sub>O<sub>4</sub> and  
430 Phase equilibria in the system Cu<sub>2</sub>O-CuO-Al<sub>2</sub>O<sub>3</sub>. *J. Am. Ceram. Soc.* 58, 192-  
431 195.

- 432 Kapoor, A., Viraraghavan, T., 1996. Discussion: Treatment of metal industrial  
433 wastewater by fly ash and cement fixation. *J. Environ. Eng.-ASCE*. 122, 243-  
434 244.
- 435 Katranitsas, A., Castritsi-Catharios, J., Persoone, G., 2003. The effects of a copper-  
436 based antifouling paint on mortality and enzymatic activity of a non-target  
437 marine organism. *Mar. Pollut. Bull.* 46, 1491-1494.
- 438 Lewis, M.A., Fischer, D.F., Murphy, C.D., 1994. Properties of glassbonded zeolite  
439 monolith. *Ceram. Trans.* 45, 277-286.
- 440 Lewis, M.A., Fischer, D.F., Smith, L.J., 1993. Salt-occluded zeolite as an  
441 immobilization matrix for chloride waste salt. *J. Am. Ceram. Soc.* 76, 2826-  
442 2832.
- 443 Li, B., Logan, B.E., 2004. Bacterial adhesion to glass and metal-oxide surfaces.  
444 *Colloid. Surface B.* 36, 81-90.
- 445 Lin, C.F., Lo, S.S., Lin, H.Y., Lee, Y., 1998. Stabilization of cadmium contaminated  
446 soils using synthesized zeolite. *J. Hazard. Mater.* 60, 217-226.
- 447 Ohlin, C.A., Villa, E.M., Rustad, J.R., Casey, W.H., 2010. Dissolution of insulating  
448 oxide materials at the molecular scale. *Nat. Mater.* 9, 11-19.
- 449 Park, D., Lee, D.S., Park, J.M., Chun, H.D., Park, S.K., Jitsuhara, I., Miki, O., Kato,  
450 T., 2005. Metal recovery from electroplating wastewater using acidophilic iron  
451 oxidizing bacteria: Pilot-scale feasibility test. *Ind. Eng. Chem. Res.* 44, 1854-  
452 1859.
- 453 Shellenberger, K., Logan, B.E., 2002. Effect of molecular scale roughness of glass  
454 beads on colloidal and bacterial deposition. *Environ. Sci. Technol.* 36,184-189.
- 455 Shih, K., Leckie, J.O., 2007. Nickel aluminate spinel formation during sintering of  
456 simulated Ni-laden sludge and kaolinite. *J. Eur. Ceram. Soc.* 27, 91-99.
- 457 Shih, K., White, T., Leckie, J.O., 2006a., Spinel formation for stabilizing simulated  
458 nickel-laden sludge with aluminum-rich ceramic precursors. *Environ. Sci.*  
459 *Technol.* 40, 5077-5083.
- 460 Shih, K., White, T., Leckie, J.O., 2006b. Nickel stabilization efficiency of aluminate  
461 and ferrite spinels and their leaching behavior. *Environ. Sci. Technol.* 40,  
462 5520-5526.
- 463 Sjollem, J., van der Mei, H.C., Uyen, H.M.W., Busscher, H.J., 1990. The influence  
464 of collector and bacterial cell surface properties on the deposition of oral  
465 streptococci in a parallel plate flow cell. *J. Adhes. Sci. Technol.* 4, 765-779.
- 466 Stumm, W., Morgan, J.J., 1996. *Aquatic Chemistry*. 3rd Ed. Wiley Interscience, New  
467 York.
- 468 Taboada-Serrano, P., Vithayaveroj, V., Yiacoumi, S., Tsouris, C., 2005. Surface  
469 charge heterogeneities measured by atomic force microscopy. *Environ. Sci.*  
470 *Technol.* 39, 6352-6360.
- 471 Teixeira da Silva, V.L.S., Lima, F.P., Dieguez, L.C., Schmal, M., 1998. Regeneration  
472 of a deactivated hydrotreating catalyst. *Ind. Eng. Chem. Res.* 37, 882-886.
- 473 Vadillo-Rodriguez, V., Logan, B.E., 2006. Localized attraction correlates with  
474 bacterial adhesion to glass and metal oxide substrata. *Environ. Sci. Technol.*  
475 40, 2983-2988.
- 476 Van Loosdrecht, M.C.M., Lyklema, L., Norde, L., Zehnder, A.J.B., 1989. Bacterial  
477 adhesion: a physicochemical approach. *Microb. Ecol.* 17, 1-15.
- 478 Wang, Y., Suryanarayana, C., An, L., 2005. Phase transformation in nanometer-sized  
479  $\gamma$ -alumina by mechanical milling. *J. Am. Ceram. Soc.* 88, 780-783.
- 480 Wartenberg, H., von Reusch, H.J., 1935. Melting diagram of refractory oxides: IV. *Z.*  
481 *Anorg. Allg. Chem.* 207, 1-20.

- 482 Wei, Y.L., Yang, Y.W., Cheng, N., 2001. Study of thermally immobilized Cu in  
483 analogue minerals of contaminated soils. *Environ. Sci. Technol.* 35, 416-421.
- 484 Wronkiewicz, D.J., Bates, J.K., Buck, E.C., Hoh, J.C., Emery, J.W., Wang, L.M.,  
485 1997. Radiation Effects in Moist-air Systems and the Influence of Radiolytic  
486 Product Formation on Nuclear Waste Glass Corrosion. Argonne National  
487 Laboratory Report No. ANL-97/15, Argonne.
- 488 Xu, Q.W., Barrios, C.A., Cutright, T., Newby, B.Z., 2005. Evaluation of toxicity of  
489 capsaicin and zosteric acid and their potential application as antifoulants.  
490 *Environ. Toxicol.* 20, 467-474.
- 491 Yousuf, M., Mollah, A., Vempati, R., Lin, T., Cocke, D., 1995. The interfacial  
492 chemistry of solidification/stabilization of metals in cement and pozzolanic  
493 material systems. *Waste Manage.* 15, 137-148.
- 494 Zhou, R.S., Snyder, R.L., 1991. Structures and transformation mechanisms of the  $\eta$ ,  $\gamma$   
495 and  $\theta$  transition aluminas. *Acta Crystallogr. B* 47, 617-630.
- 496

Fig. 1. The XRD pattern of the  $\text{CuO} + \gamma\text{-Al}_2\text{O}_3$  system shows the formation of the copper aluminate spinel when sintering at (a)  $750^\circ\text{C}$  for 3 h, and (b)  $990^\circ\text{C}$  for 20 d. The “C” represents copper oxide ( $\text{CuO}$ , ICDD PDF # 48-1548) and the “S” is for the copper aluminate spinel ( $\text{CuAl}_2\text{O}_4$ , ICDD PDF # 33-0448). The XRD pattern in (b) shows that  $\text{CuAl}_2\text{O}_4$  was the only phase in the sample and it was later used to test the  $\text{CuAl}_2\text{O}_4$  leachability.

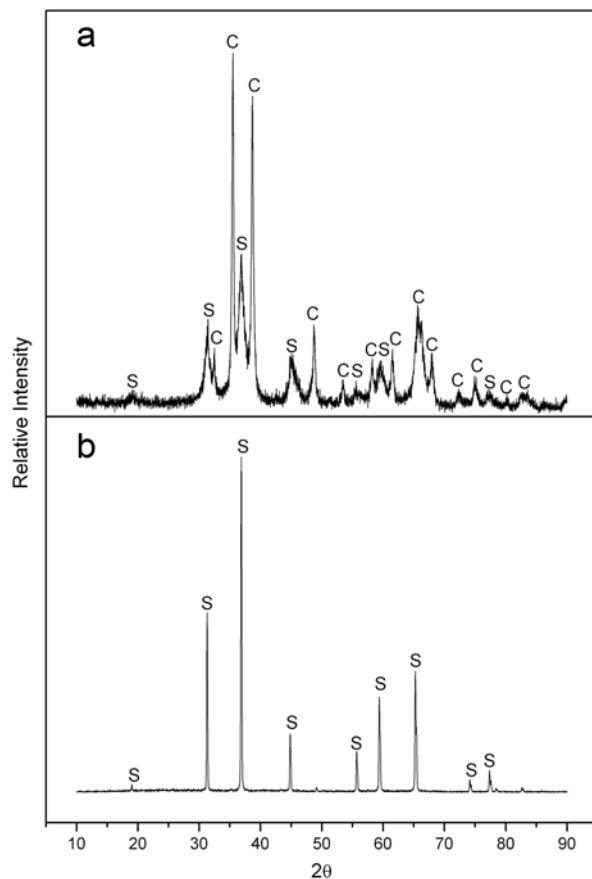


Fig. 2. The comparison of XRD patterns between (a)  $2\theta = 36.4^\circ$  and  $37.4^\circ$  (b)  $2\theta = 31.0^\circ$  and  $32.0^\circ$  for  $\text{CuO} + \gamma\text{-Al}_2\text{O}_3$  samples (with a molar ratio for Cu:Al of 1:2) sintered at 650 - 1150 °C for 3 h. The formation of  $\text{CuAl}_2\text{O}_4$  was found to reach its maximum at 1000 °C, and the curves at the top-right corners of (a) and (b) illustrate the relative intensities of the spinel peaks at  $2\theta = 36.868^\circ$  and  $2\theta = 31.294^\circ$ , respectively. The phase transformation to  $\text{CuAlO}_2$  at higher temperatures was observed by the peak at  $2\theta$  around  $31.63^\circ$ .

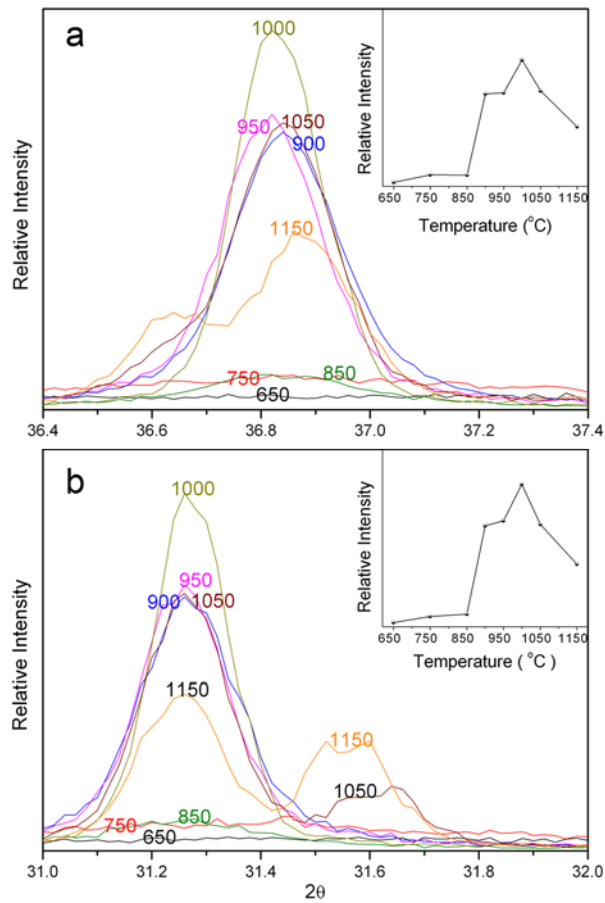


Fig. 3. The (a) pH values and (b) [Al]/[Cu] molar ratios of the leachates of the CuO and CuAl<sub>2</sub>O<sub>4</sub> phases. The leaching solution was TCLP extraction fluid no. 2 (acetic acid solution) with a pH of 2.9. Each leaching vial was filled with 10 ml of extraction fluid and 0.5 g of powder sample, and then rotated end-over-end between 0.75 and 22 d.

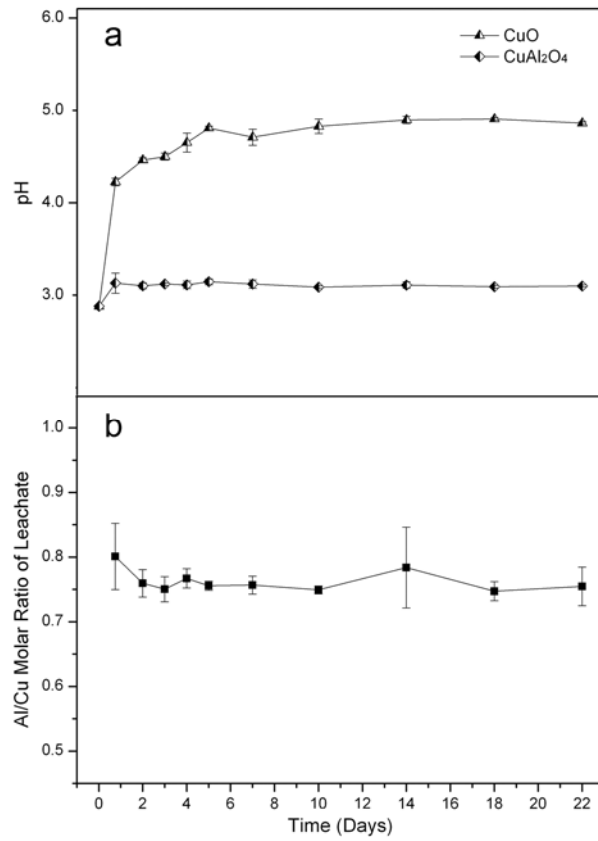


Fig. 4. Normalized copper concentrations in the leachates of CuO and CuAl<sub>2</sub>O<sub>4</sub>. The surface area of CuO powder is 0.17 m<sup>2</sup> g<sup>-1</sup> and the surface area of CuAl<sub>2</sub>O<sub>4</sub> is 1.35 m<sup>2</sup> g<sup>-1</sup>. The leaching solution was TCLP extraction fluid no. 2 (acetic acid solution) with a pH of 2.9. Each leaching vial was filled with 10 ml of extraction fluid and 0.5 g of powder samples, and then rotated end-over-end between 0.75 and 22 d. The curve in the small diagram further provides the details concerning the copper concentrations in the CuAl<sub>2</sub>O<sub>4</sub> leachate.

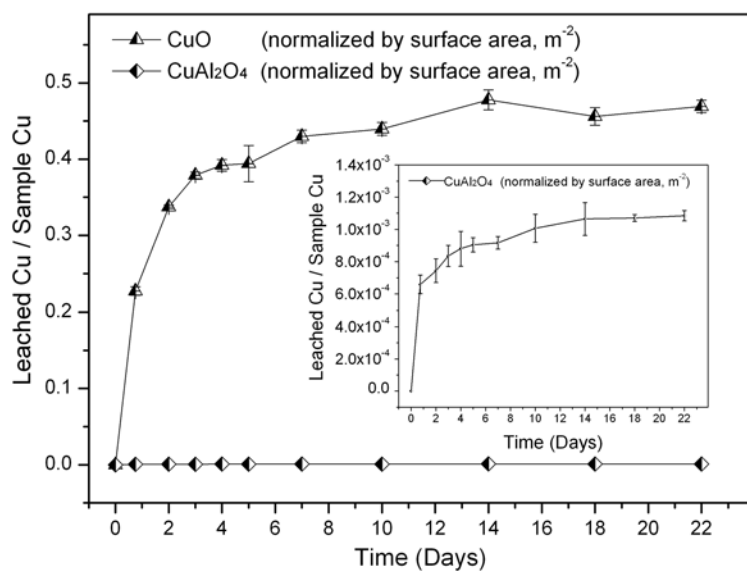


Fig. 5. The *Escherichia coli* K12 bacterial adhesion on the surface of (a) glass, (b) CuAl<sub>2</sub>O<sub>4</sub> and (c) CuO. All three materials were used as substrate and cultured for 18 h in the same solution containing *E. coli* K12 bacteria.

